J. Fluid Mech. (1981), *vol.* 108, *pp.* 101–125
Printed in Great Britain

Linear stability of rotating Hagen–Poiseuille flow

By FREDRICK W. COTTON AND HAROLD SALWEN

Department of Physics and Engineering Physics, Stevens Institute of Technology, Hoboken, N.J. 07030

(Received 26 December 1979 and in revised form 23 June 1980)

Linear stability of rotating Hagen–Poiseuille flow has been investigated by an orthonormal expansion technique, confirming results by Pedley and Mackrodt and extending those results to higher values of the wavenumber $|\alpha|$, the Reynolds number R, and the azimuthal index n. For $|\alpha| \gtrsim 2$, the unstable region is pushed to considerably higher values of R and the angular velocity, Ω. In this region, the neutral stability curves obey a simple scaling, consistent with the unstable modes being centre modes. For $n = 1$, individual neutral stability curves have been calculated for several of the low-lying eigenmodes, revealing a complicated coupling between modes which manifests itself in kinks, cusps and loops in the neutral stability curves; points of degeneracy in the R, Ω plane; and branching behaviour on curves which circle a point of degeneracy.

1. Introduction

Pedley (1969) has shown by an asymptotic approximation, valid when the wavenumber, $|\alpha|$, is low and the rotation rate, Ω, is much greater than the axial Reynolds number, R, that, for a viscous, incompressible fluid in a circular pipe, the combination of rigid-rotation and Hagen–Poiseuille flow is linearly unstable to non-axisymmetric disturbances for certain values of the parameters (R, Ω, α, and the azimuthal index n). This instability has been confirmed numerically and extended to slow rotation by Mackrodt (1976) and, independently, by us (Cotton, Salwen & Grosch 1975; Cotton 1977). These linear stability results are consistent with the global stability bound obtained by Joseph & Carmi (1969). The linear stability of this flow has also been studied in the inviscid approximation by Howard & Gupta (1962), Pedley (1968), Maslowe (1974) and Warren (1979).

In this paper, we are reporting the results of a study of the linear stability of this flow by the orthonormal expansion technique of Salwen & Grosch (1972; referred to below as I).

We have extended the neutral stability results of Mackrodt to higher $|\alpha|$, R, Ω and n. In contrast with the results in the range $0 > \alpha \gtrsim -1$, which revealed instabilities at quite low Reynolds numbers and rotation rates, we find that at $\alpha \lesssim -2$ the unstable region is pushed to considerably higher values of R and Ω. The neutral stability curves change their shape and obey a simple scaling which is consistent with the unstable modes being centre modes – small except in a region near the centre and insensitive to the radius at which the boundary conditions are imposed.

For $n = 1$, we have also calculated individual neutral stability curves for several of the low-lying eigenmodes. The results show a complicated coupling between modes

which manifests itself in kinks, cusps and loops in the neutral stability curves; points of degeneracy in the R, Ω plane at which two modes have the same complex eigenvalue; and branching behaviour on curves which circle a point of degeneracy.

2. Method of calculation

The base flow is given in physically dimensioned cylindrical co-ordinates (r^*, θ^*, z^*) by

$$\mathbf{V}^* = V_\theta^* \hat{e}_\theta + V_z^* \hat{e}_z = \Omega_0 r^* \hat{e}_\theta + W_0[1-(r^*/r_0)^2]\hat{e}_z, \tag{1}$$

where r_0 is the radius of the pipe, Ω_0 is the angular velocity and W_0 is the maximum axial velocity.

In the remainder of this paper, we shall use dimensionless variables determined by a length scale r_0, a velocity scale $V_0 = \nu/r_0$, a time scale $r_0/V_0 = r_0^2/\nu$, and a pressure scale $\rho V_0^2 = \rho\nu^2/r_0^2$, where ρ is the density and ν is the kinematic viscosity. In terms of this scaling, the base flow velocity is

$$\mathbf{V} = \Omega r \hat{e}_\theta + R(1-r^2)\hat{e}_z, \tag{2}$$

where the 'rotation rate',

$$\Omega = \Omega_0 r_0/V_0 = \Omega_0 r_0^2/\nu, \tag{3}$$

is the dimensionless angular velocity and the Reynolds number,

$$R = W_0/V_0 = r_0 W_0/\nu, \tag{4}$$

is the maximum value of the dimensionless axial velocity. (Our scaling is different from I, which used W_0 as the velocity scale. As a result, R does not appear in our equations but, instead, enters through $\mathbf{V}$, as does Ω. Also, our eigenvalues, λ_κ and σ, which will be introduced below, differ from those of I by a factor of R. Our Reynolds number, however, is the *same* as that of I.)

Our procedure is essentially the same as that of I. Because of the translational and rotational symmetry of the base flow, the linear disturbance equations,

$$\frac{\partial \mathbf{v}}{\partial t} + \nabla(\mathbf{V}\cdot\mathbf{v}) - \mathbf{v}\times(\nabla\times\mathbf{V}) - \mathbf{V}\times(\nabla\times\mathbf{v}) = -\nabla\times(\nabla\times\mathbf{v}) - \nabla p, \tag{5}$$

possess solutions of the form

$$\mathbf{v}(\mathbf{r},t) = [(u(r)\hat{e}_r + v(r)\hat{e}_\theta + w(r)\hat{e}_z]\, e^{i(n\theta+\alpha z)}\, e^{\sigma t} \tag{6}$$

for any integral n. The temporal normal modes are those for which α is real. For given R, Ω, n and α, we expand $\mathbf{v}$ in terms of the same set of expansion functions (satisfying the continuity and boundary conditions) as used in I and find that the possible σ's are the infinite, discrete set of complex eigenvalues of a matrix, $\mathbf{F}$, with elements

$$F_{kl} = \lambda_\kappa \delta_{kl} + G_{kl}, \tag{7}$$

where the λ_κ's are the real eigenvalues associated with the expansion functions (see I, equation (8)) and the matrix elements are given (I, equation (15)) by

$$G_{kl} = \langle \nabla\times(\mathbf{v}_\kappa\times\mathbf{V}) - \mathbf{v}_\kappa\times(\nabla\times\mathbf{V}), \mathbf{v}_l\rangle. \tag{8}$$

(The inner product $\langle\ \rangle$ is defined in I, equation (10).) The physical difference in this problem arises out of the fact that the velocity field (2) includes a rotational term (proportional to Ω) as well as an axial term (proportional to R).

As in I, each matrix element of $\mathbf{F}$ is expressible as a sum of a finite number of terms involving the λ_κ's, Bessel functions, and modified Bessel functions. We truncate $\mathbf{F}$ to an $M \times M$ matrix involving the M greatest (least negative) values of λ_κ, evaluate the matrix elements, and use one of several routines based upon either the QR algorithm (Wilkinson 1965; Parlett 1967) or the stabilized LR algorithm (Wilkinson 1965; IMSL 1975) to calculate the eigenvalues.

In general, not all of the eigenvalues of the truncated matrix are good approximations to eigenvalues of $\mathbf{F}$, but we have not usually been concerned with more than the first five eigenvalues; those with greatest real part, σ_r. We have generally used matrix sizes of 30×30 to 80×80 for the first three or four modes for $|\alpha| \leqslant 2$, $\Omega \leqslant 10^4$, $|\alpha| R \leqslant 10^4$ and matrix sizes up to 140×140 elsewhere, though for a few points we went as high as 180×180. The matrices were evaluated to double precision (62 bits) and, in most cases, the eigenvalue calculation used single-precision arithmetic (27 bits). As a check, we ran a number of tests of truncation error by increasing matrix size and of round-off error by using a double-precision version of the eigenvalue routine. We have shown for two test cases (Cotton 1977, §4.5) that for sufficiently large matrix size and sufficiently high arithmetic precision our numerically calculated higher eigenvalues (i.e. those with σ_r more negative) approach the corresponding diagonal matrix elements except for a residual error ('truncation edge') in the last few eigenvalues. Hence we conclude that *all* of the eigenvalues can, in principle, be determined. We have found cases of eigenvalues whose evaluation required double precision, but this was not the case for those reported in this paper.

For a given disturbance symmetry (i.e. choice of n and α), a given base flow (specified by R and Ω) will be unstable to a disturbance of that symmetry if there is at least one normal mode with positive σ_r. Then, for given n and α, the set of points with

$$\max(\sigma_r) > 0$$

defines an unstable region in the R, Ω plane. The boundary of this unstable region is the 'basic neutral stability curve' defined by $\max(\sigma_r) = 0$. Because the least stable mode (mode with maximum σ_r) at one value of (R, Ω) can change continuously to a mode which is not the least stable mode at some other point (R', Ω'), we have also found it useful to plot 'neutral stability curves' corresponding to other σ_r's going positive. All of these neutral stability curves, as well as some other special plots ($\mathrm{Re}(\sigma_1) = \mathrm{Re}(\sigma_2)$, $\mathrm{Im}(\sigma_1) = \mathrm{Im}(\sigma_2)$, or $\mathrm{Im}(\sigma) = 0$) given in § 3 below, require searching in the R, Ω plane for points whose eigenvalues have the desired properties.

It should be noted that, on any neutral stability curve, the mode for which $\sigma_r = 0$ has a real frequency and therefore is a spatial as well as temporal normal mode. The neutral stability curves presented below are, therefore, neutral stability curves for the spatial as well as the temporal problem.

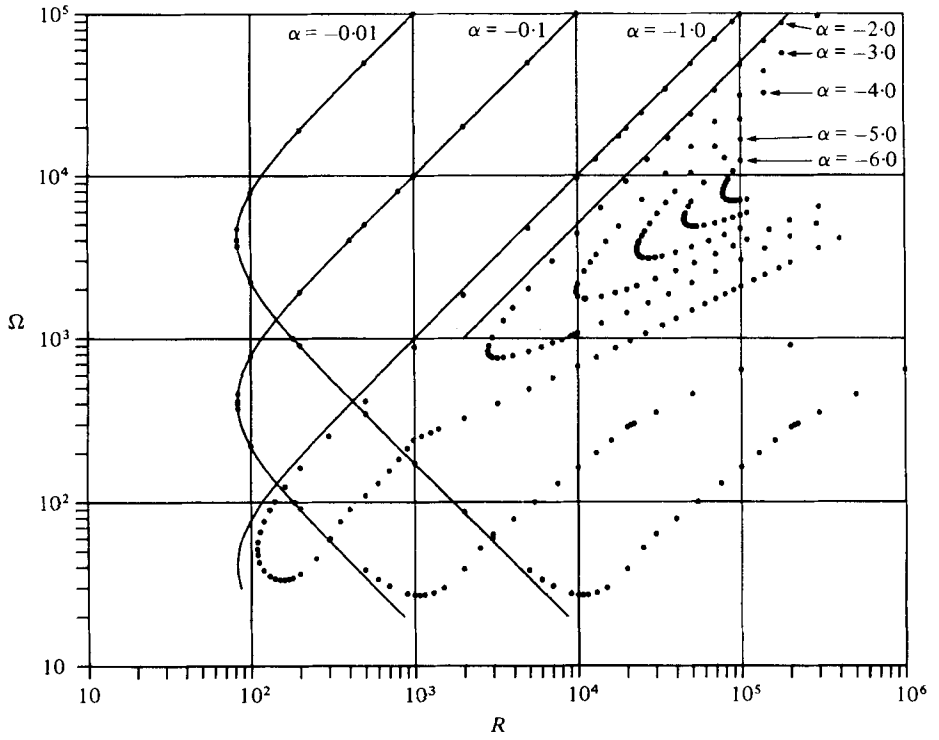

FIGURE 1. Basic neutral stability curves for rotating Hagen–Poiseuille flow, $n = 1$, selected α. The solid lines follow Pedley's approximation.

3. Results

Due to symmetry, reversal of the sign of any two of the four parameters (R, Ω, n, α) simply gives us a corresponding disturbance with the same growth or decay rate.† For convenience, we adopt the convention that R, Ω and n are non-negative while α can be positive, negative, or zero. In terms of this convention, all instabilities which have been found for this flow have been for $\alpha < 0$, which corresponds to the lines of constant phase and constant radius having the *same* screw sense as the flow lines in the base flow. For convenience, we have divided our presentation into five subsections in which we discuss the basic neutral stability curves, the neutral stability curves for the individual modes, degeneracy structure, branching behaviour, and the variation of $\mathrm{Im}(\sigma)$.

3.1. *Basic neutral stability curve. Comparison with other work*

For $n = 1, 2, 3$, we have obtained neutral stability curves for a number of different values of α. These show regularities for low $|\alpha|$ and high $|\alpha|$ and a more complicated behaviour in a transition range which is dependent on n but, in these cases, runs roughly from $\alpha = -1$ to -2. In order to show the trend with n, we also will present results for $\alpha = -1$, $n = 5$, 10, 15, and 30.

† Reversing R and α is equivalent to reversing the direction of the z axis; reversing Ω and n is equivalent to reversing the direction of x or y axis; reversing α and n is equivalent to taking the complex conjugate of the disturbance.

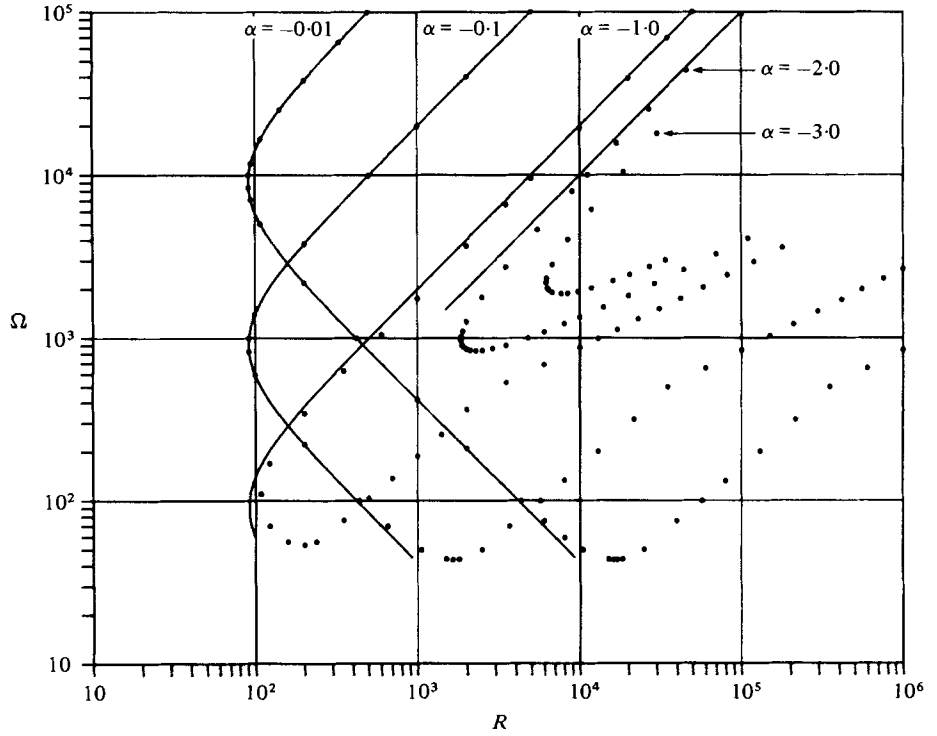

FIGURE 2. Basic neutral stability curves for rotating Hagen–Poiseuille flow, $n = 2$, selected α. The solid lines follow Pedley's approximation.

Figures 1–3 show the basic neutral stability curves for $n = 1, 2, 3$ at low and high $|\alpha|$ as well as at $\alpha = -1$, which is near the low-$|\alpha|$ end of the transition range. The curves for $\alpha = -0{\cdot}01$ and $-0{\cdot}1$ have the characteristic low-$|\alpha|$ form. At first glance, each of these appears, on these log–log plots, to be three sides of a rectangle with rounded corners, making an angle of 45° with the co-ordinate axes; on closer inspection, one sees that the bottom branch is far from straight and that its asymptotic slope is approximately $\frac{1}{2}$ ($\Omega \propto R^{\frac{1}{2}}$) rather than 1. One of the most striking properties of the low-$|\alpha|$ curves is their scaling with α which was first found by Pedley (1969) and Mackrodt (1976).

Pedley has developed a set of approximate equations for this flow, valid in the limit $\alpha \to 0$, $\Omega \to \infty$, $\alpha\Omega$ and R finite, and has found an exact solution which may be used (Cotton 1977) to derive simple equations for the neutral stability surfaces. The results are summarized in the appendix. In this approximation, the neutral stability surfaces are of the form

$$R = f_s(n, \alpha\Omega) \tag{9}$$

(where the parameter s distinguishes surfaces corresponding to different modes) and the neutral stability curves exhibit an α-independent $R_{\min}$ and the asymptotic behaviour

$$R \sim |\alpha|\,\Omega/n \quad \text{as} \quad |\alpha|\,\Omega \to \infty, \tag{10a}$$

$$R \propto (|\alpha|\,\Omega)^{-1} \quad \text{as} \quad |\alpha|\,\Omega \to 0. \tag{10b}$$

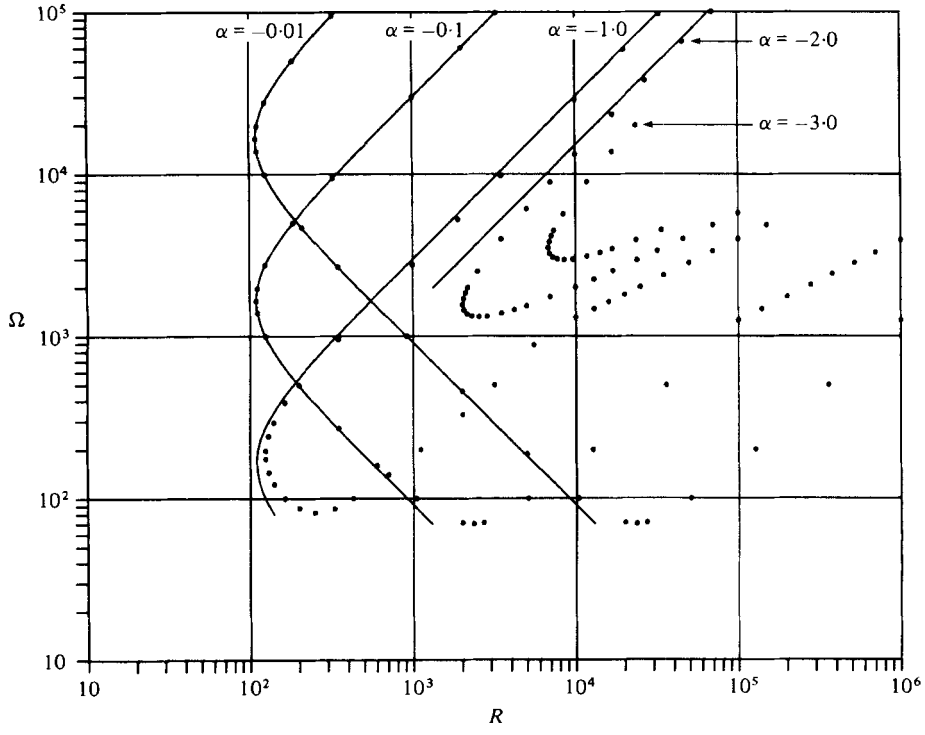

FIGURE 3. Basic neutral stability curves for rotating Hagen–Poiseuille flow, $n = 3$, selected α. The solid lines follow Pedley's approximation.

The solid curves on figures 1–3 have been calculated by using the Pedley approximation. They are in excellent agreement with our results, not only for $|\alpha| \ll 1$, $R \ll \Omega$, where it is expected, but, surprisingly, for some low-Ω sections of the $\alpha = -0{\cdot}01$ and $\alpha = -0{\cdot}1$ curves and high-R portions of the curves for higher $|\alpha|$ where $R \gtrsim \Omega$.

Mackrodt developed a set of equations which are valid for $\alpha \to 0$, $R \to \infty$, αR and Ω finite. He carried out some numerical calculations for these approximate equations as well as for the full equations for specific values of α in the range $-0{\cdot}1 \geqslant \alpha \geqslant -1{\cdot}1$. His asymptotic equations apparently cannot be integrated exactly, but they do have analogous symmetry properties to the Pedley equations which result in neutral stability surfaces of the form

$$\Omega = f_s(n, \alpha R). \tag{11}$$

Mackrodt has also shown that, in his approximation, the neutral stability curves have an α-independent $\Omega_{\min}$.

Our low-$|\alpha|$ results are in good agreement with Mackrodt's curves to the extent that we have been able to compare them and also possess the scaling property predicted by (11). (In fact, one can, for a given n, obtain our complete $\alpha = -0{\cdot}1$ curve by shifting part of the $\alpha = -0{\cdot}01$ curve downward according to (9) and part of it to the left according to (11).)

Mackrodt's numerical calculations for the full equations gave curves which start in the region where Pedley's approximation is valid and go through $\Omega_{\min}$ and along the lower branch no further than $\Omega = 200$. We are in generally good agreement with these

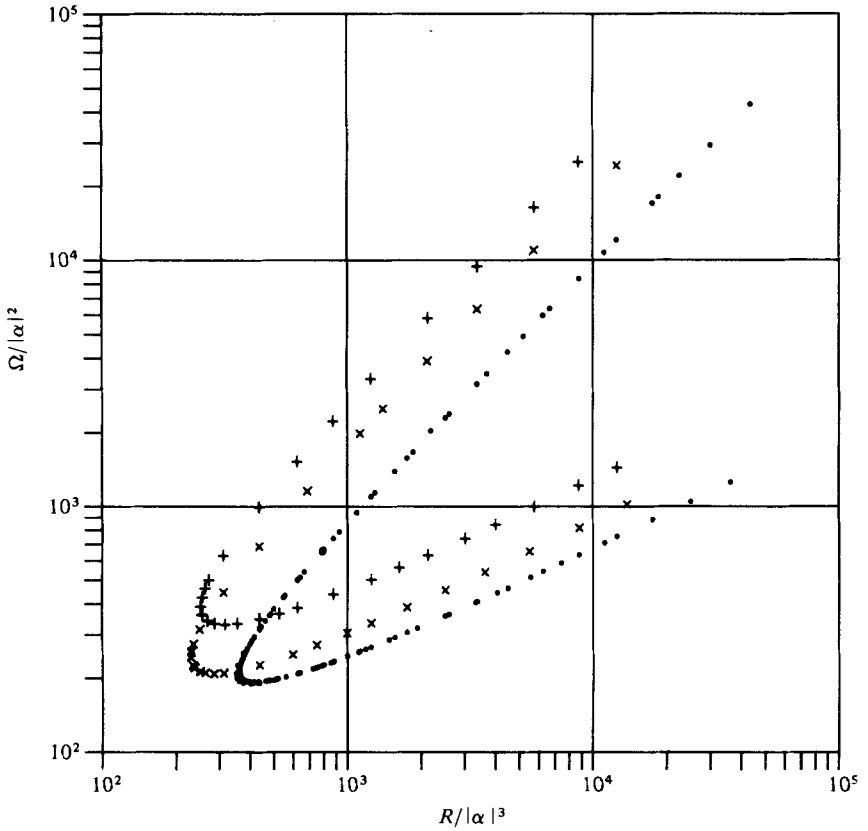

FIGURE 4. Test of high-$|\alpha|$ scaling for basic neutral stability curves for rotating Hagen–Poiseuille flow. The n values are: ., 1; ×, 2; +, 3. Note that, for $n = 1$, the $\alpha = -2{\cdot}00$ points near the nose of the curve occur at slightly lower values of $R/|\alpha|^3$, causing a spread in the curve.

results except that, for $\Omega \gtrsim 100$ on the lower branch, his $\alpha = -1{\cdot}0$ and $-1{\cdot}1$ curves have somewhat different slopes (on a log–log plot) than ours.

The neutral stability curves for $n = 1$, $\alpha = -2, -3, -4, -5, -6$ in figure 1 and for $n = 2, 3, \alpha = -2, -3$ in figures 2 and 3 show the characteristic high-$|\alpha|$ behaviour. On a log–log plot, curves for different α and the same n have the same shape but are shifted parallel to the line $R = \Omega^{\frac{3}{2}}$, with corresponding points having the same values of $R/|\alpha|^3$ and $\Omega/|\alpha|^2$. Figure 4, in which we have plotted $(\Omega/|\alpha|^2)$ *vs.* $(R/|\alpha|^3)$ for *all* of the high-$|\alpha|$ neutral stability points shown in figures 1–3, confirms that these curves have merged to form one curve for each value of n. We also find that our high-$|\alpha|$ neutral stability curves have the same asymptotic behaviour at high Reynolds number as the low-$|\alpha|$ curves:

$$|\alpha|\Omega \sim nR \quad \text{as} \quad R \to \infty \tag{12a}$$

on the upper branch and

$$\Omega \propto R^{\frac{1}{2}} \quad \text{as} \quad R \to \infty \tag{12b}$$

on the lower branch.

Figures 5–7 show the transition from low- to high-$|\alpha|$ behaviour. In a rather narrow range of α, the curves develop a constriction and pinch off to form one or more islands of instability in the low-R region and the islands then shrink and vanish. Throughout

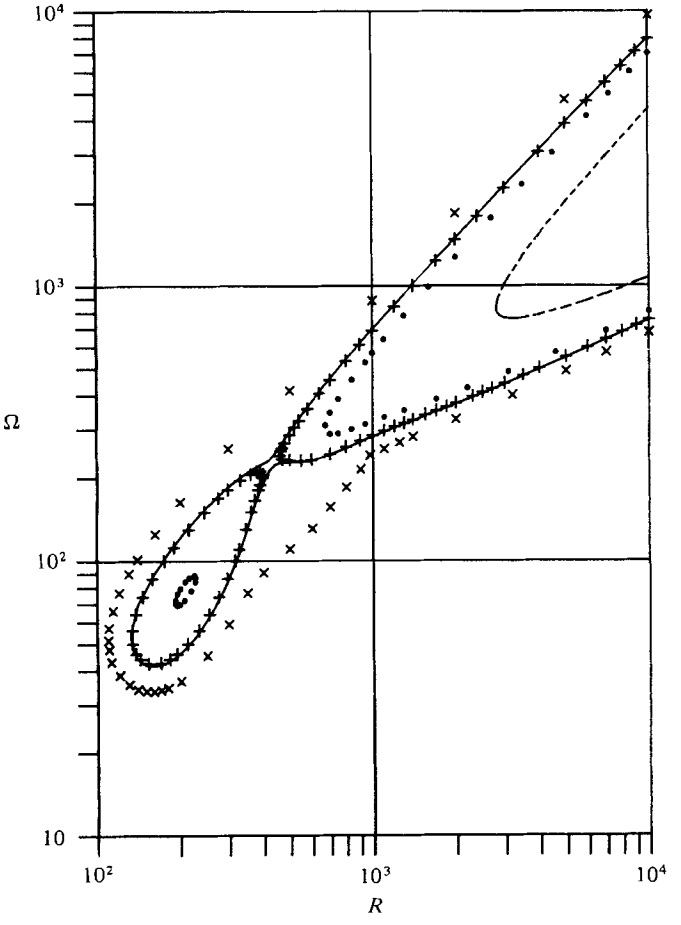

FIGURE 5. Basic neutral stability curves for rotating Hagen–Poiseuille flow, $n = 1$, selected α. The α values are: ×, $-1{\cdot}00$; solid line, $-1{\cdot}19$; +, $-1{\cdot}20$; ., $-1{\cdot}34$; dashed line, $-2{\cdot}00$.

this range of α, the form of the curves in the high-R region is quite similar to that of the high-$|\alpha|$ neutral stability curves. In particular, the asymptotic behaviour as $R \to \infty$ is given by (12) in this range of α, just as it is for low and high $|\alpha|$.

We have not carried out many calculations for $n > 3$. We do, however, present plots of the neutral stability curves for $\alpha = -1$, $n = 5, 10, 15, 30$ in figure 8 in order to show the trend with increasing n. As n increases, the unstable region for $\alpha = -1$ is pushed up to higher R and Ω but the form of the curves gets to be closer to that for low $|\alpha|$.

In table 1, we present some numerical results for points of minimum R and points of minimum Ω. The low-$|\alpha|$ minimum-Ω results are consistent with Mackrodt's results of $\Omega_{\min} = 26{\cdot}96$ at $|\alpha|R = 106{\cdot}6$ for $n = 1$ and $\Omega_{\min} = 43{\cdot}47$ at $|\alpha|R = 165{\cdot}4$ for $n = 2$. As Joseph & Carmi (1969) have noted, their stability bound, $R_c \approx 81{\cdot}49$, below which the flow must be globally stable, is remarkably close to the lowest critical Reynolds number of the linear theory (cf. our $R_{\min} \approx 82{\cdot}9$ for $n = 1$, $\alpha = -0{\cdot}01$, $\Omega = 4130$). This stability bound is, however, independent of Ω, in contrast with the linear theory, which gives no instability for $\Omega < \Omega_{\min}$.

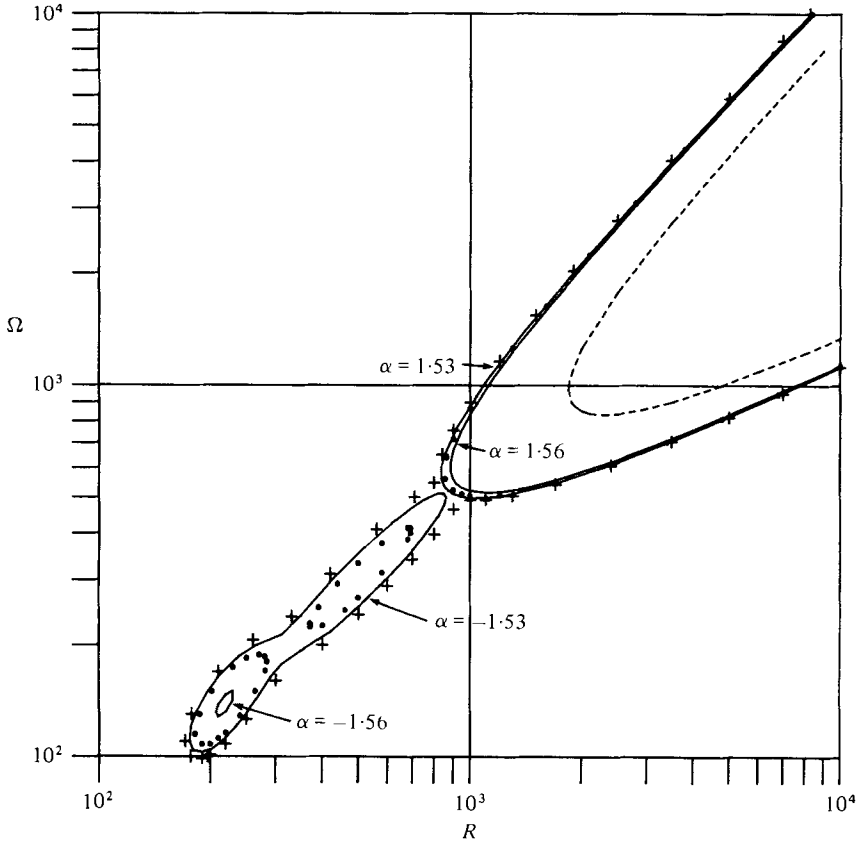

FIGURE 6. Basic neutral stability curves for rotating Hagen–Poiseuille flow, $n = 2$, selected α. The α values are: +, $-1{\cdot}52$; outer solid lines, $-1{\cdot}53$; ., $-1{\cdot}54$; inner solid lines, $-1{\cdot}56$; dashed line, $-2{\cdot}00$.

n	α	Ω_{min}	Occurs at R	R_{min}	Occurs at Ω
1	$-0{\cdot}01$	27·0	10700	82·9	4130
1	$-0{\cdot}1$	27·0	1070	83·1	415
1	$-1{\cdot}0$	33·5	156	109	51·8
1	$-2{\cdot}0$	759	3220	2810	835
2	$-0{\cdot}01$	43·5	16600	91·0	9100
2	$-0{\cdot}1$	43·5	1660	91·2	909
2	$-1{\cdot}0$	53·5	193	108	106
2	$-2{\cdot}0$	834	2280	1840	972
3	$-0{\cdot}01$	69·8	23300	110	16400
3	$-0{\cdot}1$	69·9	2330	110	1650
3	$-1{\cdot}0$	82·1	258	125	186
3	$-2{\cdot}0$	1320	2540	2020	1560
5	$-1{\cdot}0$	163	454	176	438
10	$-1{\cdot}0$	491	1510	356	1780
15	$-1{\cdot}0$	999	3650	600	4500
30	$-1{\cdot}0$	3590	20800	1680	25100

TABLE 1. Selected neutral stability data.

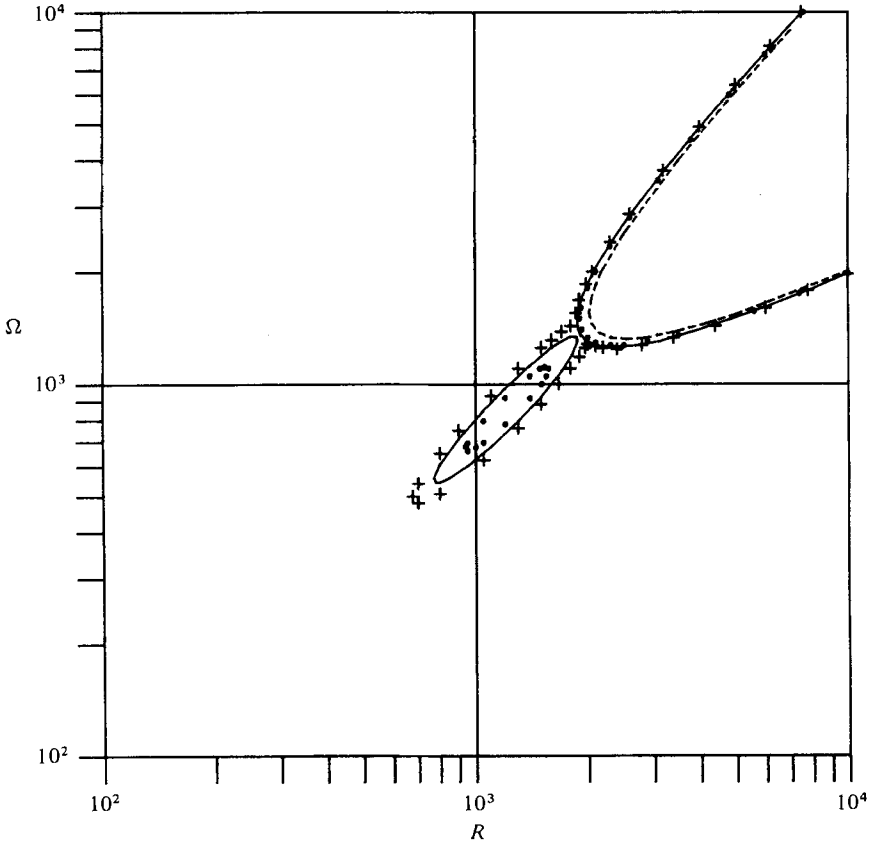

FIGURE 7. Basic neutral stability curves for rotating Hagen–Poiseuille flow, $n = 3$, selected α. The α values are: +, $-1{\cdot}94$; ——, $-1{\cdot}95$; ., $-1{\cdot}96$; – – –, $-2{\cdot}00$.

From (12), we find, for comparison with the inviscid stability results, that, for $R \to \infty$ with α and $c = R/\Omega$ fixed, the range of instability is given by $c > -\alpha/n > 0$. This agrees completely with Pedley's (1968) low-$|\alpha|$ inviscid stability results and is consistent with the necessary condition and the sufficient condition for inviscid instability derived by Maslowe (1974, equations (2.16) and (6.2)). It should be emphasized, however, that if one takes the limit of the viscous results for $R \to \infty$ at fixed Ω, the flow will be stable.

3.2. *Higher modes*

Some of the most interesting behaviour was discovered when we decided to look at the neutral stability curves for the higher eigenmodes for $n = 1$ and to compare them with the appropriate Pedley limits. Figures 9–13 show some of these curves at various values of α.

For $\alpha = -0{\cdot}1$ (figure 9), the behaviour in the region of Pedley's study is very regular. Outside of this region, however, there are changes in the order of the real part of σ for the different modes and corresponding crossings of the neutral stability curves. In particular, the crossing of the curves designated as mode 1 and mode 2 gives rise to a kink in the basic neutral stability curve which was visible in figure 1.

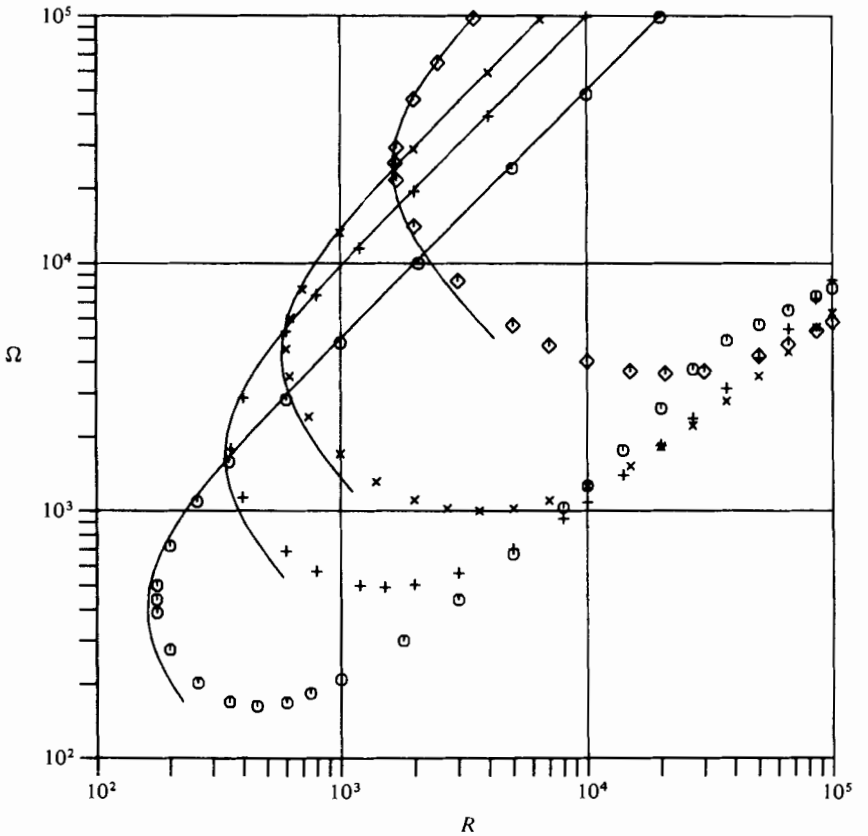

FIGURE 8. Basic neutral stability curves for rotating Hagen–Poiseuille flow, $\alpha = -1{\cdot}00$, selected n. The n values are: ⊙, 5; +, 10; ×, 15; ◇, 30. The solid lines follow Pedley's approximation.

For $\alpha = -0{\cdot}9$ (figure 10), the neutral stability curves for the two least-stable modes have formed a cusp (at $R = 1550$, $\Omega = 871$) and matching indentation which suggest a more complicated behaviour. In addition, the neutral stability curves for the third and fourth modes have shifted to higher values of R and Ω and now resemble the high-$|\alpha|$ form discussed in § 3.1. At $\alpha = -0{\cdot}909$ (figure 11), the low-R parts of the two curves have joined (near the former position of the cusp) to form a closed loop and the 'tails' of the two curves have joined at the low-R end and have approached each other at the high-R end. Inside the loop and between the tails, there are *two* unstable modes. Since the loop at $\alpha = -0{\cdot}909$ has been formed from pieces of what were two separate mode curves at $\alpha = -0{\cdot}9$, it is clear that the mode labelling has to be revised. We have chosen a local ordering in which the most unstable mode is defined to be mode 1, etc. (see figure 11).

By $\alpha = -1{\cdot}0$ (figure 12), the loop is somewhat smaller and the tails have either disappeared or moved to higher R and Ω. The curve (with $R_{\min}$ close to 10^4) which we labelled as the mode 3 neutral stability curve for $\alpha = -0{\cdot}9$ (figure 10) now corresponds to mode 2. Inside it, as well as inside the loop, there are two unstable modes. By $\alpha = -1{\cdot}1$ (circles on figure 13), the loop has shrunk almost to vanishing; by $\alpha = -1{\cdot}15$ (solid line on figure 13) the loop has disappeared.

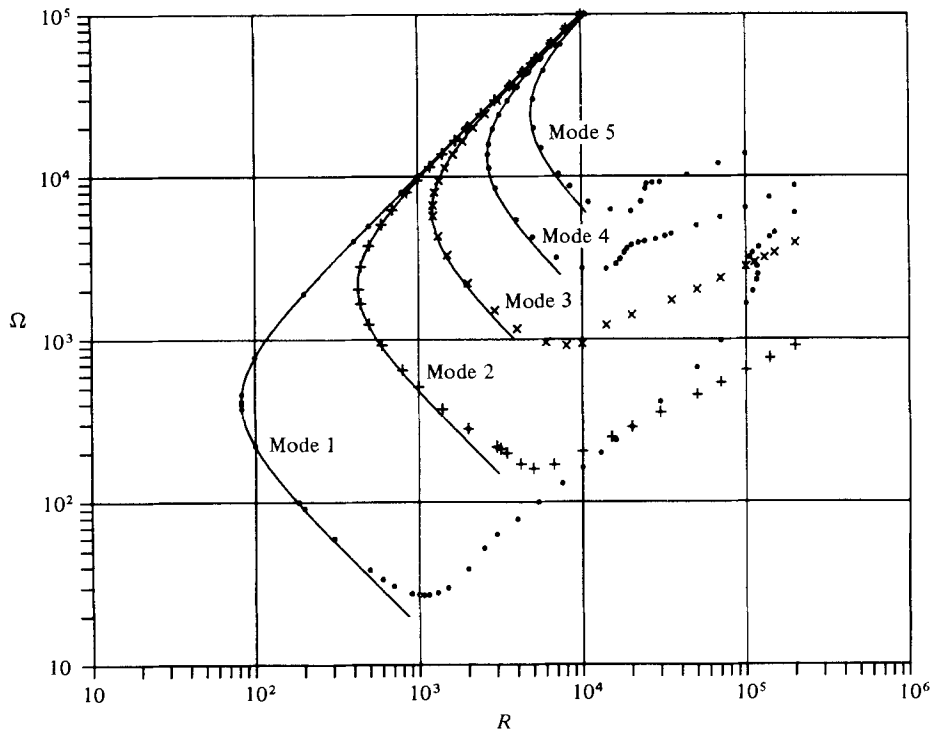

FIGURE 9. Neutral stability curves for the first five eigenmodes, $n = 1$, $\alpha = -0{\cdot}100$. The solid lines follow Pedley's approximation.

3.3. *Degeneracy structure*

At the crossing point of the loop (indicated by arrow on figure 12), there are two neutrally stable ($\sigma_r = 0$) modes with different values of σ_i. Since, on the remainder of the loop, one of the two modes is unstable and the other is neutrally stable, the crossing-point is the *only* point on the loop where the two modes have equal σ_r. We also found *one* point on the loop where the two modes have equal σ_i. That suggested that the locus of equal σ_r and the locus of equal σ_i each enter the loop without leaving and this led us to investigate those curves.

The results for $\alpha = -1{\cdot}0$ are shown in figure 14. The curves defined by

$$\mathrm{Re}(\sigma_1) = \mathrm{Re}(\sigma_2) \quad \text{and} \quad \mathrm{Im}(\sigma_1) = \mathrm{Im}(\sigma_2)$$

meet at two points of degeneracy (i.e. $\sigma_1 = \sigma_2$), ($R \approx 296$, $\Omega \approx 33{\cdot}8$) and ($R \approx 563$, $\Omega \approx 343$), and appear to form a single smooth curve. One of the points of degeneracy lies just inside the loop; the other is in the stable region.

To investigate whether, at the points of degeneracy, there are two linearly independent eigenfunctions corresponding to the same eigenvalue or one eigenfunction and one generalized eigenfunction (see, e.g., Di Prima & Habetler 1969), we calculated

$$\cos\theta_{12} = \frac{|(v_1, v_2)|}{[(v_1, v_1)(v_2, v_2)]^{\frac{1}{2}}}, \tag{13}$$

the cosine of the 'angle' between the numerical eigenvectors for the two least-stable modes, at the values of (R, Ω) corresponding to our best numerical estimates of the

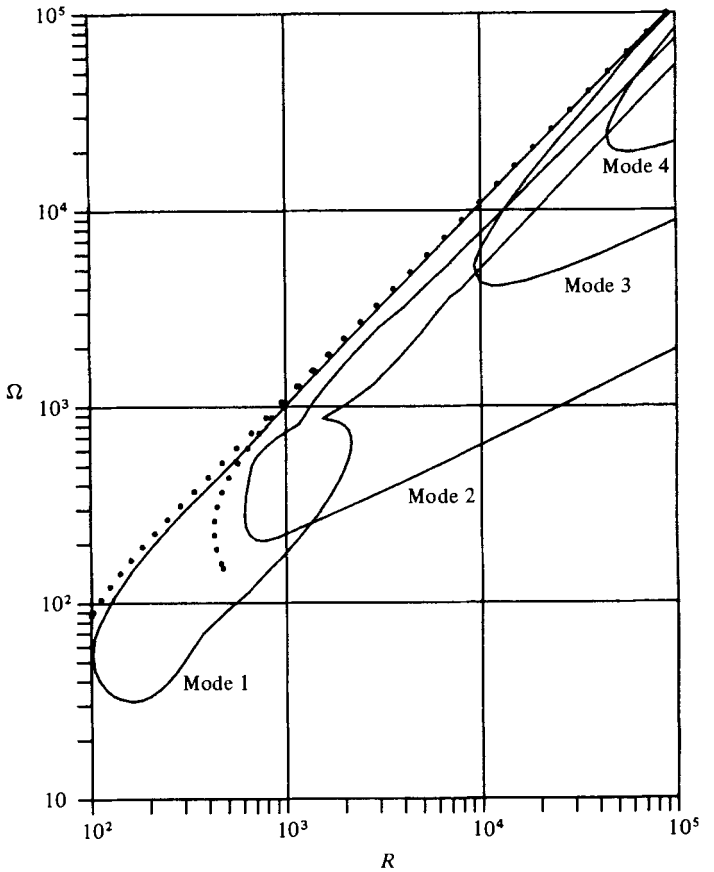

FIGURE 10. Neutral stability curves for the first four eigenmodes, $n = 1$, $\alpha = -0{\cdot}900$. The dots (.) follow Pedley's approximation for the first two modes; for modes 3 and 4, the approximation is too inaccurate to be relevant.

points of degeneracy. The cosines obtained were 0·99917 at the lower point and 0·99965 at the upper point. These values lead us to believe that $\cos\theta_{12} \to 1$ at the actual points of degeneracy, which corresponds to having one eigenvector and one generalized eigenvector. In later work, we have found similar behaviour for a degeneracy in non-rotating Hagen–Poiseuille flow (Salwen, Cotton & Grosch 1980).

The degeneracy structure continues to exist at both lower and higher $|\alpha|$. Figures 15–17 show the loci of equal real and imaginary parts of σ_1 and σ_2 for a number of different values of α, ordered in sequence from low $|\alpha|$ to high $|\alpha|$. At $\alpha = -0{\cdot}1$ (figure 15), we find only one point of degeneracy (in the stable region at $R \approx 2310$, $\Omega \approx 31{\cdot}0$) and the curves of equal σ_r and of equal σ_i give no indication of joining at the upper end. Figure 16 shows part of the transition from an open to a closed locus. By $\alpha = -0{\cdot}9$, the structure is much the same as that at $\alpha = -1{\cdot}0$, even though the stability loop has not yet closed. Figure 17 shows the disappearance of the degeneracy structure at higher $|\alpha|$. When the stability loop vanishes ($\alpha = -1{\cdot}15$), the upper point of degeneracy is forced into the stable region. By $\alpha = -1{\cdot}25$, these two points of degeneracy have merged and disappeared and the remaining loop, given entirely by $\sigma_{1r} = \sigma_{2r}$, is close to disappearing.

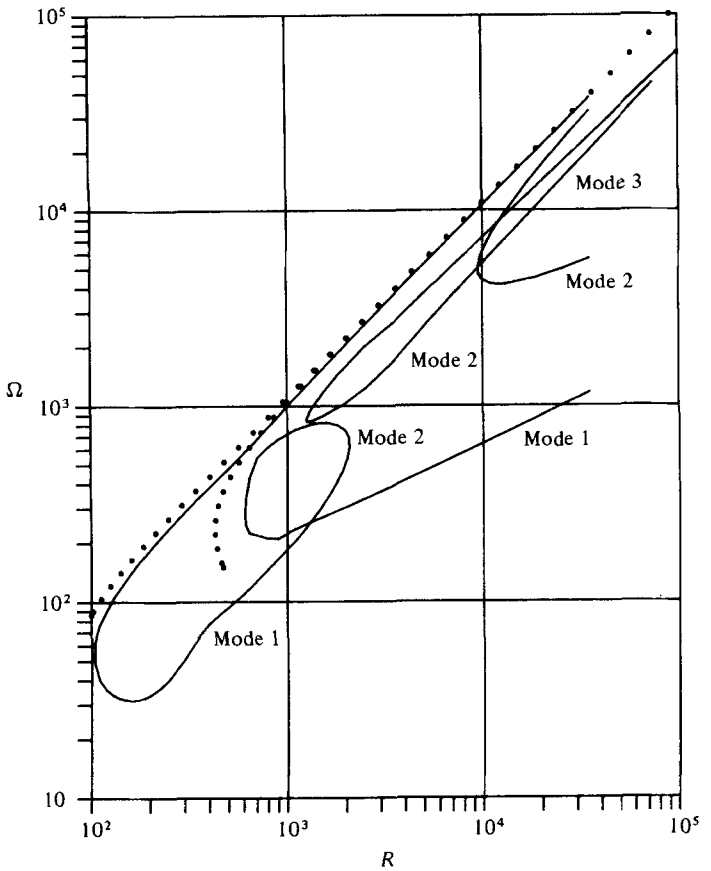

FIGURE 11. Neutral stability curves for the first three eigenmodes, $n = 1$, $\alpha = -0{\cdot}909$. The dots (.) follow Pedley's approximation for the first two modes; the approximation for mode 3 is too inaccurate to be relevant.

3.4. *Branching behaviour*

Because the eigenvalues are continuous functions of α, R and Ω, our initial inclination was to number the modes by a continuous mapping from their order in the Pedley region (σ_1 least stable in the Pedley region, σ_2 next least stable, ..., with $\sigma_1, \sigma_2, \ldots$ continuous complex functions). We discovered, however, that the two modes we numbered σ_1 and σ_2 interchanged values in circling the stability loop of figure 14, so that this numbering system could not be unique. At the crossing point both modes are neutrally stable, with $\mathrm{Re}(\sigma_1) = \mathrm{Re}(\sigma_2) = 0$, $\mathrm{Im}(\sigma_1) = \sigma_{1i}$, $\mathrm{Im}(\sigma_2) = \sigma_{2i} + \sigma_{1i}$. As one goes around the loop in the counter-clockwise direction, one is following a neutrally stable mode with $\mathrm{Im}(\sigma)$ initially equal to σ_{1i} and an unstable mode with $\mathrm{Im}(\sigma)$ initially equal to σ_{2i} and both modes have continuous real and imaginary parts. When one arrives back at the crossing, $\mathrm{Im}(\sigma)$ for the *neutrally* stable mode approaches σ_{2i} and $\mathrm{Im}(\sigma)$ for the *unstable* mode approaches σ_{1i}, so they have interchanged eigenvalues.

This interchange will occur on any loop which circles one of the points of degeneracy and not the other. As the loop crosses the segment $\mathrm{Re}(\sigma_1) = \mathrm{Re}(\sigma_2)$, the real parts of the eigenvalues change order; as the loop crosses $\mathrm{Im}(\sigma_1) = \mathrm{Im}(\sigma_2)$ the imaginary parts change order; in a full circuit of the loop, both real and imaginary parts change

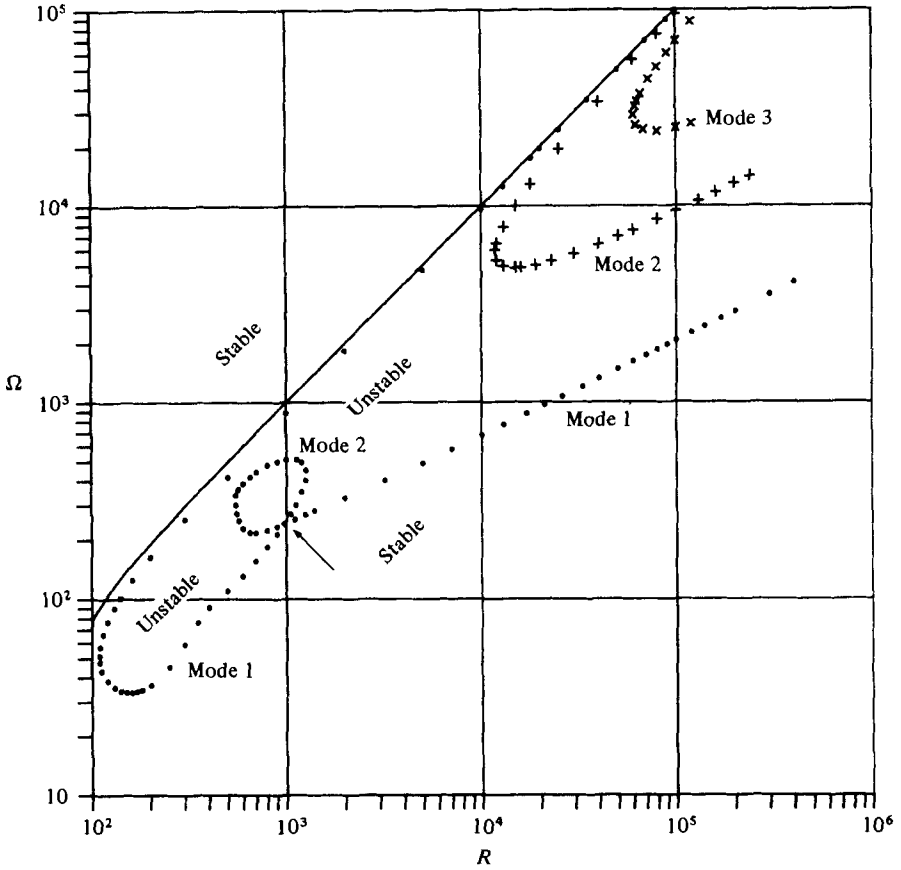

FIGURE 12. Neutral stability curves for the first three eigenmodes, $n = 1$, $\alpha = -1{\cdot}00$. The solid line follows Pedley's approximation for the first mode; the approximation for mode 2 (not shown in figure) fails to show any loop structure. Inside the loop, there are two unstable modes. The arrow points to the location of the crossing point of the loop.

order so the values of σ_1 and σ_2 are interchanged. In circling a loop which encloses *both* points of degeneracy (or none) the eigenvalues are not interchanged. Interchanges of eigenvalues occur for any closed path enclosing a single point of degeneracy regardless of the form of the neutral stability curves.

The branching behaviour of these two eigenvalues in the R, Ω plane is analogous to that of a complex function with a double-sheeted Riemann surface and a pair of branch points. The present phenomenon is, however, much more complicated. There is a matching pair of degeneracies with R and $\Omega < 0$; there are indications in the results (e.g. additional crossings) of more degeneracies which would couple these modes to other normal modes; and it is even possible that *all* the modes are coupled, pairwise, in this manner.

We have received from Dr P.-A. Mackrodt a copy of an earlier report (Mackrodt 1971) than the one (Mackrodt 1976) referred to above. Mackrodt found branching on one curve and suspected it was connected with a Riemann sheet behaviour associated with some sort of singular point. He did not, however, identify the singular point

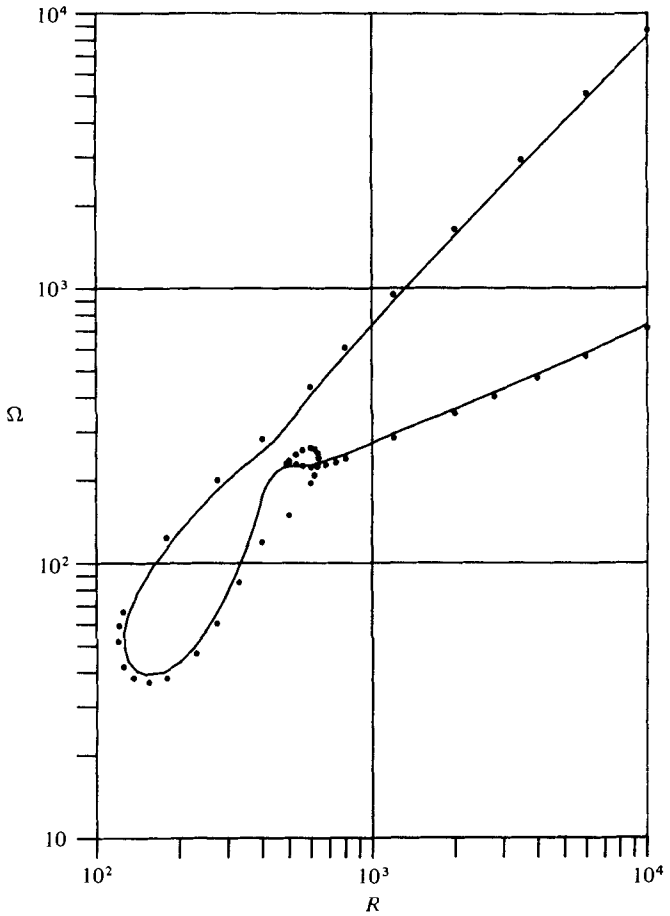

FIGURE 13. Neutral stability curves for the first two eigenmodes, $n = 1$, $\alpha = -1{\cdot}10$ and for the first eigenmode for $\alpha = -1{\cdot}15$. The curve for $\alpha = -1{\cdot}15$ has been shown as a solid line to distinguish it easily from the curve for $\alpha = -1{\cdot}10$. Inside the loop for $\alpha = -1{\cdot}10$, there are two unstable modes.

(which in this case was the degeneracy in the stable region) and, therefore, was unable to predict accurately the circumstances in which such branching should be expected.

3.5. *Results for* $\mathrm{Im}(\sigma)$

For all of the cases studied, we find

$$\mathrm{Im}(\sigma) \approx -n\Omega - \alpha R \approx -n\Omega\left(1-\frac{\alpha^2}{n^2}\right) \tag{14}$$

on the high-R portion of the upper branch of the neutral stability curve, which is consistent with Pedley's conclusion that $\mathrm{Im}(\sigma) \approx -n\Omega$ for $\alpha \to 0$. (The two forms of the right-hand side of (14) are equivalent because of the asymptotic variation (12a) of R with Ω.) We have not found any simple generalization for $\mathrm{Im}(\sigma)$ on the remainder of the neutral stability curves except that, in all cases, $\mathrm{Im}(\sigma) > 0$ on the high-R portion of the lower branch.

Thus, for $|\alpha| \lesssim n$, $\mathrm{Im}(\sigma)$ changes from negative values on the upper branches to

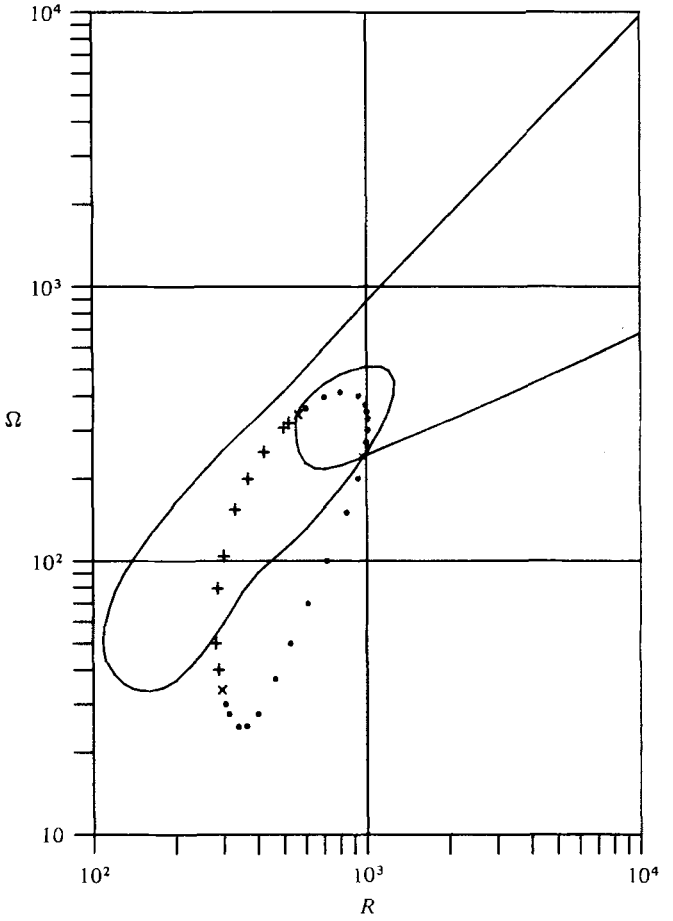

FIGURE 14. Lines of $\mathrm{Re}(\sigma_1) = \mathrm{Re}(\sigma_2)$ and $\mathrm{Im}(\sigma_1) = \mathrm{Im}(\sigma_2)$, $n = 1$, $\alpha = -1{\cdot}00$. +, $\mathrm{Im}(\sigma_1) = \mathrm{Im}(\sigma_2)$; ., $\mathrm{Re}(\sigma_1) = \mathrm{Re}(\sigma_2)$; ×, $\sigma_1 = \sigma_2$, degeneracy. The solid line follows the neutral stability curve for modes 1 and 2.

positive values on the lower branches of the neutral stability curves and we can expect to find curves of $\mathrm{Im}(\sigma) = 0$. On each of these curves, the disturbance with $\mathrm{Im}(\sigma) = 0$ is a 'standing wave' in the sense that its phase,

$$\phi(\theta, z, t) \equiv n\theta + \alpha z + \mathrm{Im}(\sigma)t, \tag{15}$$

is independent of the time. Figure 18 shows portions of the standing wave lines in the unstable region for two modes at $n = 1$, $\alpha = -0{\cdot}1$. As expected from the above discussion, the standing-wave lines move out of the unstable region at $\alpha \approx -n$. Figure 19 shows a portion of the standing-wave line for the most unstable mode at $n = 1$, $\alpha = -1$; it lies just below the upper branch of the neutral stability curve. The standing-wave lines for the other $n = 1$, $\alpha = -1{\cdot}0$ modes (not shown) lie in the stable region just above the upper branch of the neutral stability curve.

At the point of intersection of the standing-wave curve for a particular mode with the neutral stability curve for that mode, $\sigma = 0$ so the disturbance is time-independent. Table 2 is a listing of some points for which $\sigma = 0$.

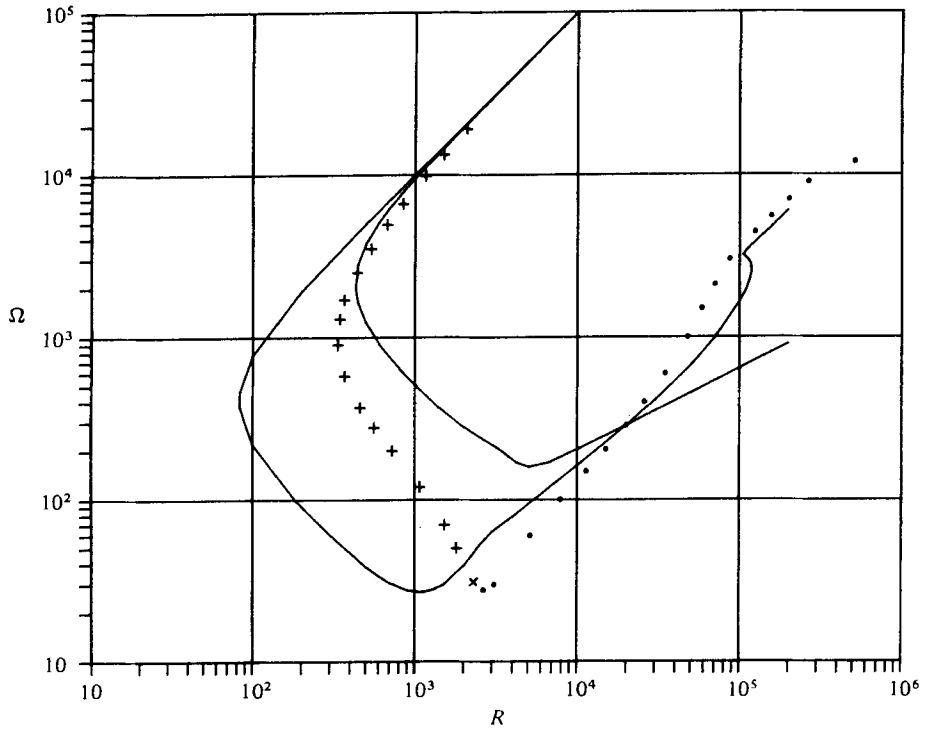

FIGURE 15. Lines of $\mathrm{Re}(\sigma_1) = \mathrm{Re}(\sigma_2)$ and $\mathrm{Im}(\sigma_1) = \mathrm{Im}(\sigma_2)$, $n = 1$, $\alpha = -0{\cdot}100$. +, $\mathrm{Im}(\sigma_1) = \mathrm{Im}(\sigma_2)$; ., $\mathrm{Re}(\sigma_1) = \mathrm{Re}(\sigma_2)$; ×, $\sigma_1 = \sigma_2$, degeneracy. The solid lines follow the neutral stability curves for modes 1 and 2.

n	α	Mode	R	Ω
1	−0·1	1	599	33·8
1	−0·1	2	3160	211
1	−1·0	1	162	125

TABLE 2. Points of intersection of standing-wave lines with their respective neutral stability curves ($\sigma = 0$).

The usual definition, $-\mathrm{Im}(\sigma)/\alpha R$, for the phase speed yields (as can be seen from (14) and the fact that α is negative) a large *negative* phase speed in the region of validity of the Pedley approximation. Instead, we define

$$c = -(\sigma + in\Omega)/(i\alpha R) \tag{16}$$

so that

$$\phi = n(\theta - \Omega t) + \alpha(z - Rc_r t), \tag{17}$$

where c_r is the real part of c. With this definition, we find that c_r lies between 0 and 1 in the region studied, as it does for non-rotating Poiseuille flow.

From (14), it can be seen that each of the unstable modes we have studied is a fast mode (i.e. $c \to 1$ as $R \to \infty$) near the upper branch of its neutral stability curve. It is also true that, for $|\alpha| \gtrsim 1$, all unstable modes have $c_r \sim 1$ in the high-R region. We have not been able to rule out the possibility that some of the modes with $|\alpha| < 1$ are

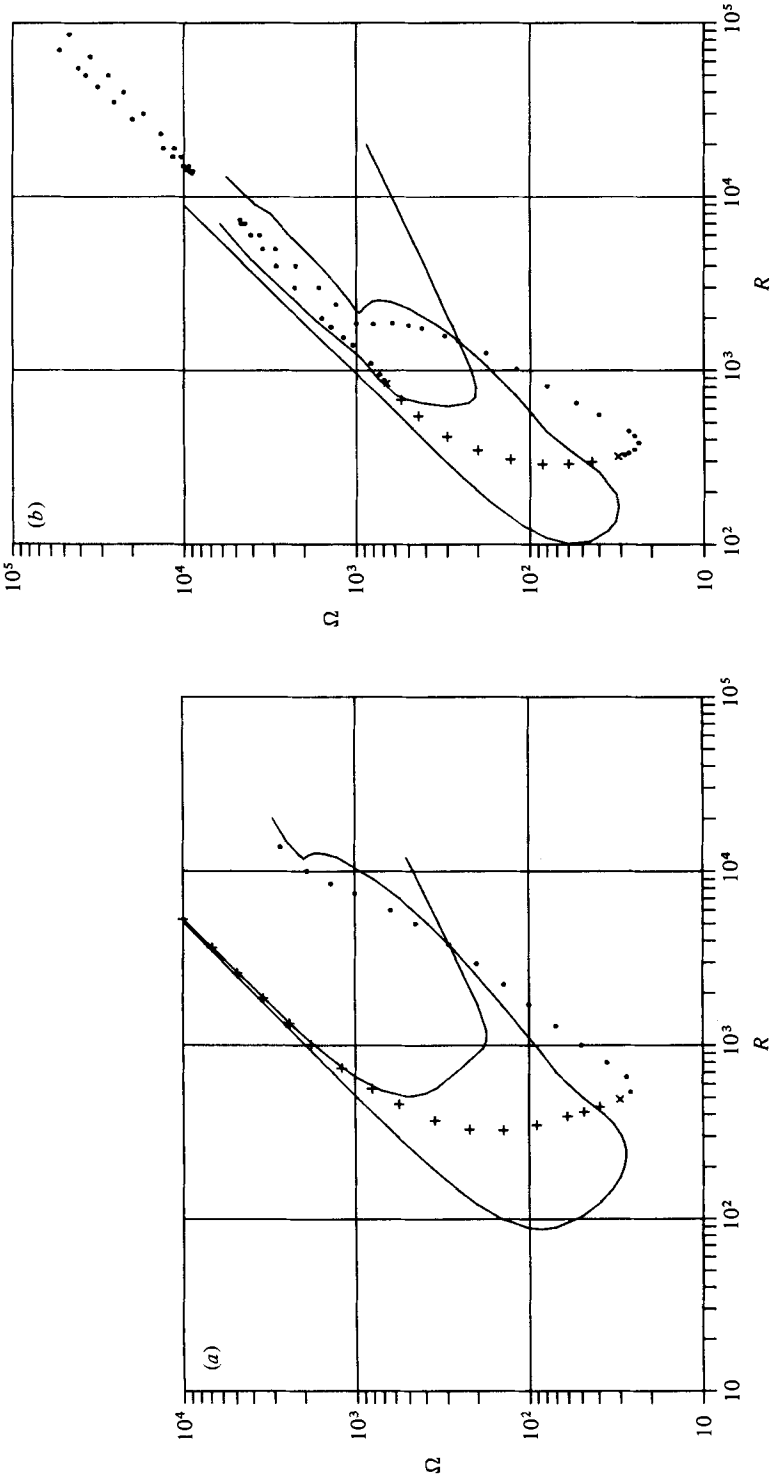

FIGURE 16 (*a*, *b*). For legend see next page.

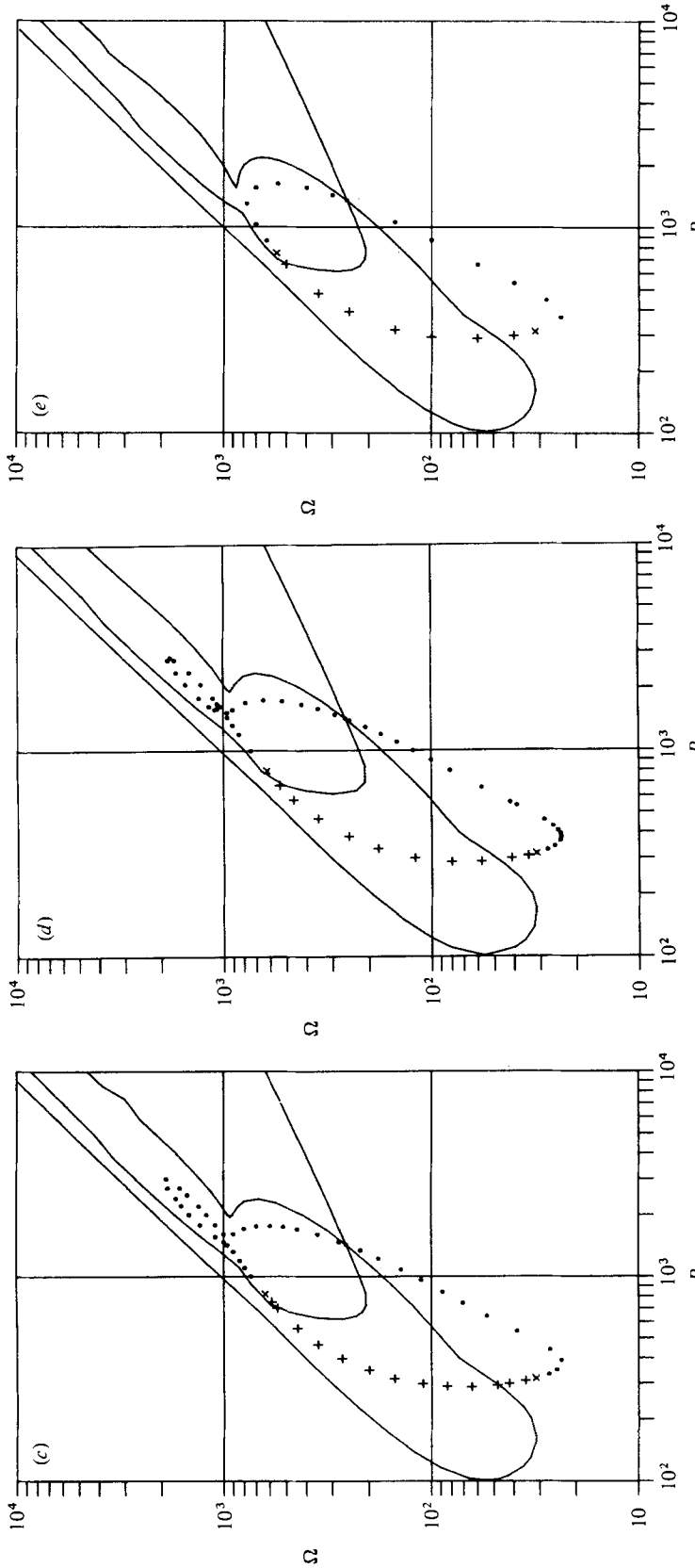

FIGURE 16. Lines of $\mathrm{Re}(\sigma_1) = \mathrm{Re}(\sigma_2)$ and $\mathrm{Im}(\sigma_1) = \mathrm{Im}(\sigma_2)$, $n = 1$, selected α. +, $\mathrm{Im}(\sigma_1) = \mathrm{Im}(\sigma_2)$; ·, $\mathrm{Re}(\sigma_1) = \mathrm{Re}(\sigma_2)$; ×, $\sigma_1 = \sigma_2$, degeneracy. The solid lines follow the neutral stability curves for modes 1 and 2. (*a*) $\alpha = -0{\cdot}500$; (*b*) $\alpha = -0{\cdot}868$; (*c*) $\alpha = -0{\cdot}880$; (*d*) $\alpha = -0{\cdot}881$; (*e*) $\alpha = -0{\cdot}900$.

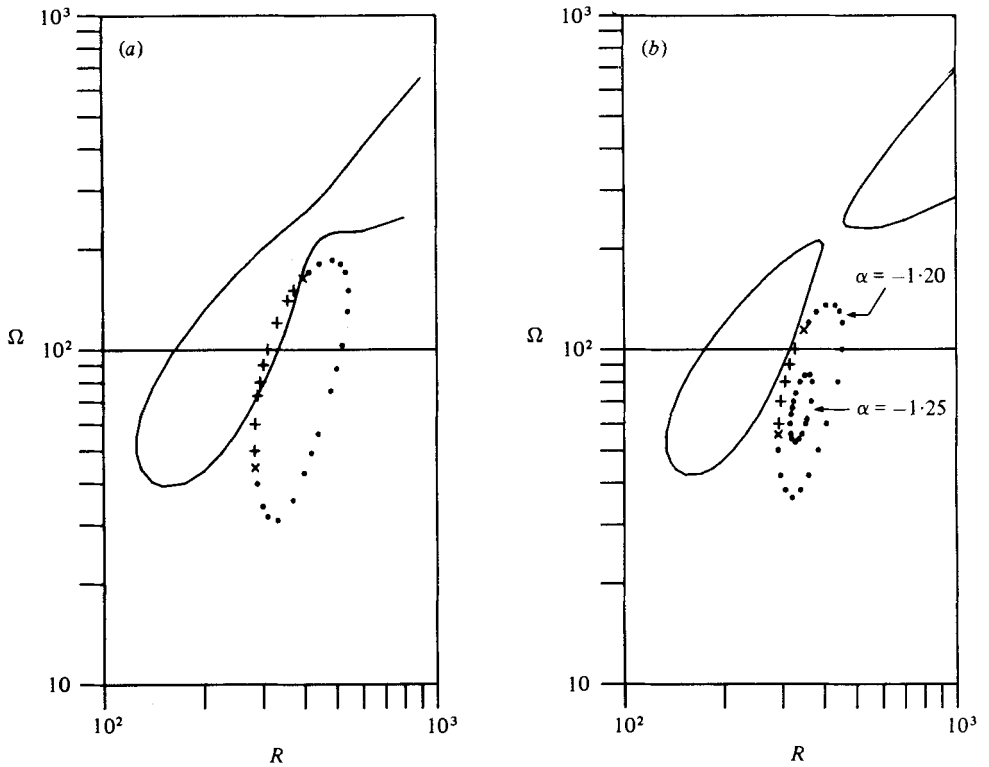

FIGURE 17. (*a*) Lines of $\mathrm{Re}(\sigma_1) = \mathrm{Re}(\sigma_2)$ and $\mathrm{Im}(\sigma_1) = \mathrm{Im}(\sigma_2)$, $n = 1$, $\alpha = -1{\cdot}15$. +, $\mathrm{Im}(\sigma_1) = \mathrm{Im}(\sigma_2)$; ., $\mathrm{Re}(\sigma_1) = \mathrm{Re}(\sigma_2)$; ×, $\sigma_1 = \sigma_2$, degeneracy. The solid line follows the basic neutral stability curve. (*b*) Lines of $\mathrm{Re}(\sigma_1) = \mathrm{Re}(\sigma_2)$, $\mathrm{Im}(\sigma_1) = \mathrm{Im}(\sigma_2)$, $n = 1$, $\alpha = -1{\cdot}20$, and $\mathrm{Re}(\sigma_1) = \mathrm{Re}(\sigma_2)$, $n = 1$, $\alpha = -1{\cdot}25$. +, $\mathrm{Im}(\sigma_1) = \mathrm{Im}(\sigma_2)$; ., $\mathrm{Re}(\sigma_1) = \mathrm{Re}(\sigma_2)$; ×, $\sigma_1 = \sigma_2$, degeneracy. The solid line follows the basic neutral stability curve for $\alpha = -1{\cdot}20$.

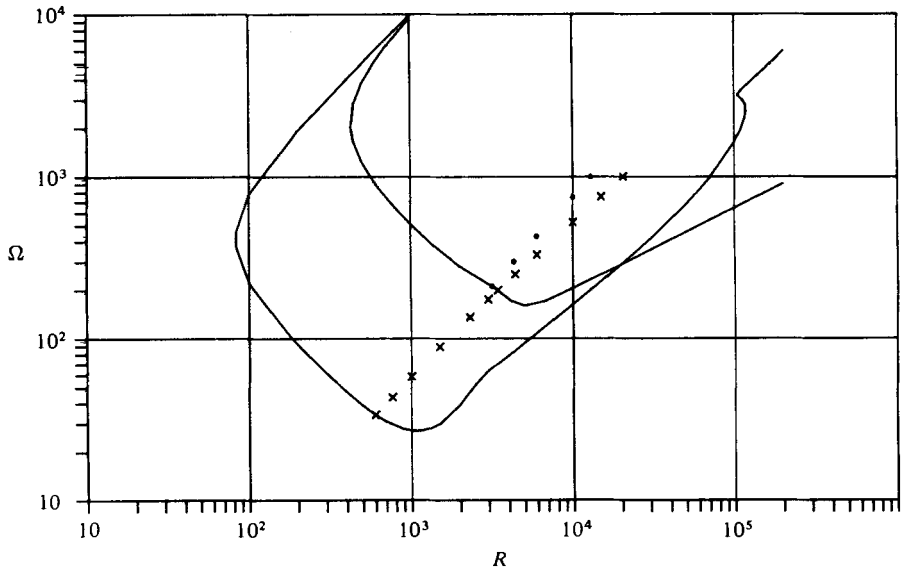

FIGURE 18. Standing-wave lines, $n = 1$, $\alpha = -0{\cdot}100$. Only that portion of the standing-wave line which is within the region of instability has been shown. The solid line follows the neutral stability curve for modes 1 and 2.

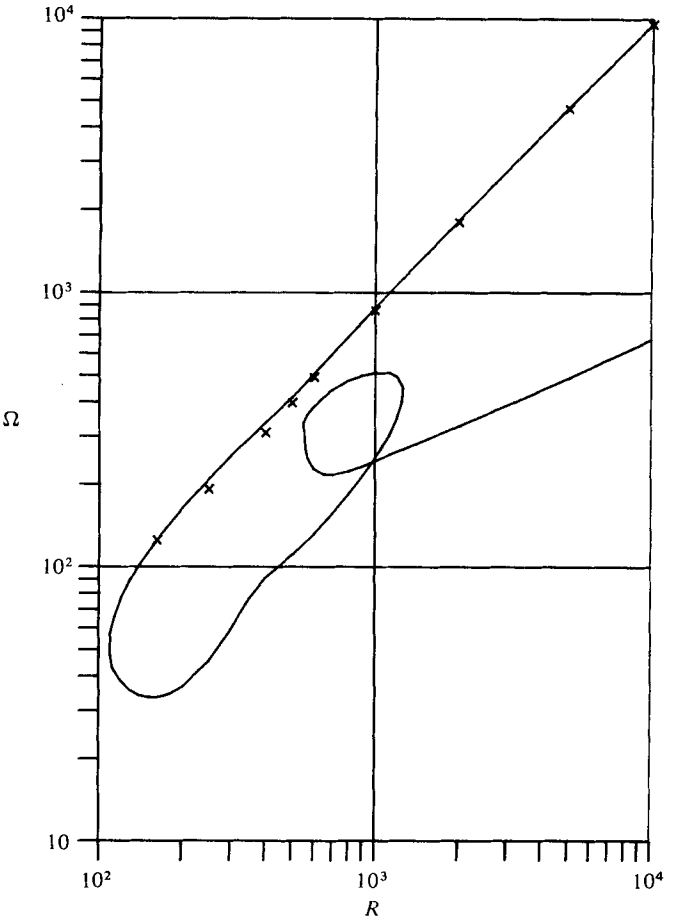

FIGURE 19. Standing-wave line, $n = 1$, $\alpha = -1{\cdot}00$. Only that portion of the standing-wave line which is within the region of instability has been shown. The solid line follows the neutral stability curve for modes 1 and 2.

slow modes ($c \to 0$ as $R \to \infty$) near the lower branches of their neutral stability curves. On the high-$|\alpha|$ neutral stability curves, we find that $(\sigma + in\Omega + i\alpha R)/|\alpha|^2$ is roughly independent of α for fixed n, $R/|\alpha|^3$ and $\Omega/|\alpha|^2$.

4. Centre-mode scaling

For
$$\alpha \lessgtr 0, \tag{18}$$

the rescaling
$$\xi = |\alpha| r = \mp \alpha r, \tag{19a}$$
$$\tilde{p} = p/|\alpha| = \mp p/\alpha, \tag{19b}$$
$$\lambda = (\sigma + in\Omega + i\alpha R)/\alpha^2 \tag{19c}$$

puts the continuity equation, $\nabla \cdot \mathbf{v} = 0$, in the form

$$\frac{1}{\xi}\frac{d}{d\xi}(\xi u) + \frac{in}{\xi} v \mp i w = 0 \tag{20}$$

and the momentum equation (5) in the form

$$(\lambda \pm iR'\xi^2)u - 2\Omega' v + \frac{d\tilde{p}}{d\xi} = \frac{1}{\xi}\frac{d}{d\xi}\left(\xi\frac{du}{d\xi}\right) - \left(\frac{n^2+1}{\xi^2}+1\right)u - \frac{2in}{\xi^2}v, \tag{21a}$$

$$(\lambda \pm iR'\xi^2)v + 2\Omega' u + \frac{in}{\xi}\tilde{p} = \frac{1}{\xi}\frac{d}{d\xi}\left(\xi\frac{dv}{d\xi}\right) - \left(\frac{n^2+1}{\xi^2}+1\right)v + \frac{2in}{\xi^2}u, \tag{21b}$$

$$(\lambda \pm iR'\xi^2)w - 2R'\xi u \mp i\tilde{p} = \frac{1}{\xi}\frac{d}{d\xi}\left(\xi\frac{dw}{d\xi}\right) - \left(\frac{n^2}{\xi^2}+1\right)w, \tag{21c}$$

where

$$R' = \frac{R}{|\alpha|^3} = \frac{r_0 W_0}{\nu|\alpha^* r_0|^3} = -\frac{1}{2\nu|\alpha^*|^3}\frac{d^2V_z^*}{dr^{*2}}\bigg|_0 = \frac{1}{\nu|\alpha^*|}\left[V_z^*(0) - V_z^*\left(\frac{1}{|\alpha^*|}\right)\right], \tag{22a}$$

$$\Omega' = \frac{\Omega}{|\alpha|^2} = \frac{\Omega_0 r_0^2}{\nu|\alpha^* r_0|^2} = \frac{1}{\nu|\alpha^*|^2}\frac{dV_\theta^*}{dr^*}\bigg|_0 = \frac{1}{\nu|\alpha^*|}\left[V_\theta^*\left(\frac{1}{|\alpha^*|}\right) - V_\theta^*(0)\right], \tag{22b}$$

and $\alpha^* = \alpha/r_0$ is the unscaled wavenumber. The equations now involve n, R', and Ω' but no separate α. The parameter α now appears only in the boundary conditions, which become

$$u = V = W = 0 \quad \text{at} \quad \xi = |\alpha|. \tag{23}$$

(The upper sign in equations (19)–(21) corresponds to the case of negative α, for which we present results in this paper.)

This rescaling of the equations can account for the scaling of the high-$|\alpha|$ neutral stability curves (figure 4) and for the insensitivity of $\mathrm{Im}(\lambda)$ to α for fixed n, R' and Ω' (§ 3.5) if the solutions are insensitive to the radius, $\xi = |\alpha|$, at which the boundary conditions (23) are applied. This seems to indicate that these disturbances are 'centre modes' for which the disturbance velocity falls off rapidly with radius and is already small for $r \ll 1$.

5. Discussion

Mackrodt (1976) constructed an envelope of the neutral stability curves for different α and confirmed, by experiments on a long pipe, that this is the correct stability boundary for this flow. It is remarkable that a small amount of rigid rotation makes Hagen–Poiseuille flow unstable to long-wavelength disturbances. This result suggests that it may be important to study the effects of swirling (rotation in the central portion which does not extend to the wall) on the stability of flow in a non-rotating pipe. At the very least, any experimental study of pipe-flow stability should include an estimate of the amount of swirling which is present.

The scaling of the neutral stability curves appears to indicate (§4) that, at least for high $|\alpha|$, the unstable modes are centre modes. This result is in contrast to plane Poiseuille flow (Lin 1955) where the unstable modes are wall modes.

There are indications in our numerical results of a large number of degeneracies in addition to the ones we have studied. The coupling of modes associated with these degeneracies may have important effects on the accuracy of approximate calculations in the affected regions of the R, Ω plane.

We wish to thank Mr William Torman and Mr Obed Duardo who spent many hours running most of our more recent results. This research could not have been carried out without the generous assistance of the SIT Computer Center.

s	$\zeta_s(1)$
1	4·36
2	7·54
3	10·70
4	13·87
5	16·99

TABLE 3. Values of $\zeta_s(1)$.

Appendix

From Pedley's (1969) results, it is possible to derive the equation of the neutral stability curve, in his limit, to be

$$4\alpha^2\Omega^2 + 4\alpha n\Omega R + \zeta_s^6(n) = 0. \tag{A 1}$$

The parameter $\zeta_s(n)$, which he denoted by $\mu_s(n)$, is the sth eigenvalue ($s = 1, 2, 3, \ldots$) of his equations (4.5) and (4.8a). For $s = 1$, Pedley calculated values of ζ for $1 \leqslant n \leqslant 10$ iteratively (see his table 1) and developed an empirical formula accurate to three significant figures for $n \geqslant 6$ (his equations (5.4) and (5.5)).

Using the standard asymptotic formulas for the Bessel functions of complex argument, we have approximated his eigenvalue equation by

$$\left(-2\sqrt{3}+\frac{6}{\zeta_s}(n^2-\tfrac{1}{4})\right)\tan\phi - 6 + \frac{1}{\zeta_s}\left(2n^2\sqrt{3}-\frac{\sqrt{3}}{2}\right) = 0, \tag{A 2}$$

where $\phi = \zeta_s - \frac{1}{2}(n+\frac{1}{2})\pi$ (see Cotton 1977, 4.2.13). This should be valid for the very high modes for any n; it is valid for all the modes for $n = 1$. We have calculated iteratively the values $\zeta_s(1)$, $1 \leqslant s \leqslant 5$ (see table 3). The asymptotic solution of equation (A 2),

$$\zeta_s(n) \sim \tfrac{1}{2}(n-\tfrac{1}{6})\pi + s\pi,$$

gives an error of 2 % for $\zeta_1(1)$ and 0·3 % for $\zeta_3(1)$.

REFERENCES

COTTON, F. W. 1977 A study of the linear stability problem for viscous incompressible fluids in circular geometries by means of a matrix–eigenvalue approach. Ph.D. dissertation, Stevens Institute of Technology. (University Microfilms International, Ann Arbor, MI. 48106, order no. 77–26,931.)

COTTON, F. W., SALWEN, H. & GROSCH, C. E. 1975 *Bull. Am. Phys. Soc.* **20**, 1416.

DI PRIMA, R. C. & HABETLER, G. J. 1969 *Arch. Rat. Mech.* **34**, 218–227.

HOWARD, L. N. & GUPTA, A. S. 1962 *J. Fluid Mech.* **14**, 463–476.

IMSL 1975 *IMSL Library* 2, 5 edn. International Mathematical and Statistical Libraries, Inc., 7500 Bellaire Blvd, Houston, TE. 77036.

JOSEPH, D. D. & CARMI, S. 1969 *Quart. Appl. Math.* **16**, 575–599.

LIN, C. C. 1955 *The Theory of Hydrodynamic Stability*. Cambridge University Press.

MACKRODT, P.-A. 1971 *Stabilität von Hagen-Poiseuille-Strömungen mit überlagerter starrer Rotation*. Mitteilungen aus dem Max-Planck-Institut für Strömungsforschung und der Aerodynamischen Versuchsanstalt (Nr. 55), Göttingen.

MACKRODT, P.-A. 1976 *J. Fluid Mech.* **73**, 153–164.

MASLOWE, S. A. 1974 *J. Fluid Mech.* **64**, 307–317.

PARLETT, B. N. 1967 The LR and QR algorithms. In *Mathematical Methods for Digital Computers*, vol. II (ed. A. Ralston & H. S. Wilf). Wiley.

PEDLEY, T. J. 1968 *J. Fluid Mech.* **31**, 603–607.

PEDLEY, T. J. 1969 *J. Fluid Mech.* **35**, 97–115.

SALWEN, H., COTTON, F. W. & GROSCH, C. E. 1980 *J. Fluid Mech.* **98**, 273–284.

SALWEN, H. & GROSCH, C. E. 1972 *J. Fluid Mech.* **54**, 93–112.

WARREN, F. W. 1979 *Proc. Roy. Soc.* A **368**, 225–237.

WILKINSON, J. H. 1965 *The Algebraic Eigenvalue Problem.* Oxford University Press.